

Detachment of semiflexible polymer chains from a substrate - a Molecular Dynamics investigation

J. Paturej^{1,2}, A. Erbas³, A. Milchev⁴, and V.G. Rostiashvili⁵

¹ *Leibniz-Institut of Polymer Research Dresden, 01069 Dresden, Germany*

² *Institute of Physics, University of Szczecin, Wielkopolska 15, 70451 Szczecin, Poland*

³ *Department of Materials Science and Engineering,
Northwestern University, Evanston, IL 60208, USA*

⁴ *Institute for Physical Chemistry Bulgarian Academy of Sciences, 1113 Sofia, Bulgaria*

⁵ *Max-Planck-Institute for Polymer Research, Ackermannweg 10, 55128 Mainz, Germany*

Using Molecular Dynamics simulations, we study the force-induced detachment of a coarse-grained model polymer chain from an adhesive substrate. One of the chain ends is thereby pulled at constant speed off the attractive substrate and the resulting saw-tooth profile of the measured mean force $\langle f \rangle$ vs height D of the end-segment over the plane is analyzed for a broad variety of parameters. It is shown that the observed characteristic oscillations in the $\langle f \rangle$ - D profile depend on the bending and not on the torsional stiffness of the detached chains. Allowing for the presence of hydrodynamic interactions (HI) in a setup with explicit solvent and DPD-thermostat, rather than the case of Langevin thermostat, one finds that HI have little effect on the $\langle f \rangle$ - D profile. Also the change of substrate affinity with respect to the solvent from solvophilic to solvophobic is found to play negligible role in the desorption process. In contrast, a changing ratio $\epsilon_s^B/\epsilon_s^A$ of the binding energies of A- and B-segments in the detachment of an AB-copolymer from adhesive surface strongly changes the $\langle f \rangle$ - D profile whereby the B-spikes vanish when $\epsilon_s^B/\epsilon_s^A < 0.15$. Eventually, performing an atomistic simulation of (bio)-polymers, we demonstrate that the simulation results, derived from our coarse-grained model, comply favorably with those from the all-atom simulation.

I. INTRODUCTION

During the last decade a rapid development of the so-called single molecule dynamic force spectroscopy (SMDFS) has enabled the direct observation of the chemical dissociation (e.g., base-pair binding in DNA, or ligand-receptor interaction in proteins) initiated by an external time-dependent force in the pico-Newton range [1–3]. Theoretical interpretation of SMDFS for a single bond rupture has been suggested by Bell [5], and developed by Evans [6, 7]. The Bell-Evans (BE) approach is built upon an Arrhenius relationship which describes the bond rupture rate (“off”-rate) subject to a time-dependent force, $k_{\text{off}} = \kappa_0 \exp(x_\beta f/k_B T)$, where κ_0 denotes the rupture rate in the absence of applied force, f is the applied force per bond, and x_β is the coordinate where the activation barrier is located. Here and in what follows, T denotes the temperature, and k_B is the Boltzmann constant. In other words, the effective activation energy is represented as a linear function of the force, $E_b(f) = E_b^{(0)} - x_\beta f$. Under the condition of fixed loading rate, $f = \mathcal{R}t$, it could be shown that $f = (k_B T/x_\beta) \ln(\mathcal{R}x_\beta/\kappa_0 k_B T)$, i.e., the detachment force grows linearly with the logarithm of loading rate \mathcal{R} . This relationship is usually referred to as the Bell-Evans model and employed for the measurement of dynamic strength of molecular bonds, cells’ adhesion, and protein unfolding by means of an atomic force microscopy (AFM) [8]. However, for multiply bonded attachments the f vs $\ln \mathcal{R}$ relationship shows a non-linear behavior which might be related to a more complicated cascade of activation barriers [9].

A single-stranded DNA (ssDNA), strongly adsorbed on a graphite substrate, represents an example of a multiply-bonded bio-assembly. The desorption of such tethered DNA molecule, induced by the applied force, has been first studied by Jagota *et al.* [10–13]. At equilibrium, the macromolecule can be desorbed either by using the displacement of the chain end over the adsorbing surface (and measuring the fluctuating force), or by fixing the pulling force, applied to the chain end, and monitoring the mean displacement of the end segment over the plane. It has been shown (analytically and by means of Brownian simulation) that in the displacement control (DC) desorption, the average force $\langle f \rangle$ - displacement D profile exhibits a characteristic set of saw-tooth (force-spikes) oscillations, corresponding to the underlying base sequence of the ssDNA [10–13].

When the displacement profile reaches a steady state, i.e., the desorbed monomers are far away from both ends of the chain, each maximum in the saw-tooth oscillations corresponds to an energy barrier that has to be overcome in order to complete the monomer desorption. In a real system, this energy barrier, G_b , is quite complex and composed of various energetic and entropic contributions. For instance, interaction energy between monomers and the surface, G_{surf} , conformational entropic contributions and enthalpic energies of polymer chains G_{conf} , contributions due to direct additive interactions and entropic effects of water molecules near the surface, or with the chain G_{sol} , etc. One may assume that these energetic components can be decoupled, and the overall energy barrier can be expressed as $G_b \approx G_{\text{surf}} + G_{\text{conf}} + G_{\text{sol}} + G_{\text{other}}$, where G_{other} represents all contributions that cannot be accessed by a coarse-grained

(CG) simulation model (such as hydrogen bonding of water molecules near/around the monomers). In that case, using Molecular Dynamic (MD) simulations, effects of various contributions on the polymer-surface interactions as well as non-equilibrium single molecule experiments can be tackled systematically and in detail.

Recently we have revisited the detachment theory of a strongly adsorbed macromolecule by making use of a free-energy-based stochastic equation (the so called Onsager equation) approach, and by performing extensive Molecular Dynamic (MD) simulations [14]. This study has confirmed the force-spikes response under DC and also demonstrated how the saw-tooth profile is smeared out with growing detachment velocity v_c and increasing mass of the AFM-cantilever. Moreover, we have shown that the average detachment force versus detachment velocity v_c relationship exhibits a *nonlinear* behavior when plotted in semilogarithmic coordinates. The presence of fluctuations in our model enables, among other things, to calculate the probability distribution function (PDF) of the fluctuating force at the cantilever, measured at the moment of ultimate detachment, which is an experimental observable in laboratory studies.

In the present paper we extend and generalize our previous MD simulations [14] so as to probe systematically the influence of various energy contributions to the desorption energy barrier G_b , more precisely, on the resulting force $\langle f \rangle$ - displacement D profiles. Using a CG model, the pairwise interactions between monomers can be tuned to understand their influence on displacement profiles. Similarly, by introducing torsional and dihedral harmonic potentials in addition to the classic bead-spring potentials (further details on the simulations scheme will be given below), effects of bending and/or torsional stiffness of the polymer backbone on the detachment behavior are examined. At this point we should also note that the energy components forming the overall energy barrier G_b can be in phase with each other along the reaction coordinate (distance above the substrate in this case). Hence, their addition can make an energy minimum between two consecutive maxima more shallow or deeper as we will see later in this paper.

The paper is organized as follows. First, in Section II we examine the role of hydrodynamic interactions within the context of external force-driven polymer desorption by comparing the effect of Langevin- and DPD thermostats within our coarse-grained (CG) model. We also check the role of substrate wettability and its impact on the $\langle f \rangle$ - D profile. Then, the desorption of an alternating $A - B$ copolymer with different binding energies of the A - and B -monomers to the substrate is examined. In addition, the effect of bending and/or torsional stiffness of the polymer backbone on the detachment behavior is studied. Eventually, in Section III we report on atomistic MD simulation of polypeptide detachment, using poly-glycin and poly-phenylalanine, adsorbed on a crystalline carbon substrate, and compare it to the generic behavior of our coarse-grained model. Our report ends with a brief summary, presented in Section IV.

II. COARSE-GRAINED SIMULATIONS

A. Model

Similar to our previous study [14], simulations of a coarse-grained model were carried out based on a generic bead-spring model of a flexible polymer chain [15], composed of N monomers, connected by nonlinear bonds along the polymer backbone. The bonded (two-body) interactions in the chain is described by the Kremer-Grest [15] potential, $V^{\text{KG}}(r) = V^{\text{FENE}}(r) + V^{\text{LJ}}(r)$ with the so-called “finitely extensible nonlinear elastic” (FENE) potential given by

$$V^{\text{FENE}} = -\frac{1}{2}kr_0^2 \ln \left[1 - \left(\frac{r}{r_0} \right)^2 \right] \quad (1)$$

The non-bonded interactions between monomers were taken into account by means of the Lennard-Jones (LJ) potential, given by:

$$V^{\text{LJ}}(r) = 4\epsilon \left[(\sigma/r)^{12} - (\sigma/r)^6 + 1/4 \right] \theta(r_c - r). \quad (2)$$

In Eqs. (1) and (2), $r = |\mathbf{r}_{ij}|$ denotes the distance between the center of monomer (bead) i and j , r_c is the cutoff distance, while the energy scale ϵ and the length scale σ are chosen as the units of energy and length, respectively. Accordingly, the remaining parameters are fixed at the values $k = 30\epsilon/\sigma^2$ and $r_0 = 1.5\sigma$ [15]. In Eq. (2) we have introduced the Heaviside step function $\theta(x) = 0$ or 1 for $x < 0$ or $x \geq 0$. We performed simulations with short- and long-range cutoff: $r_c = 2^{1/6}\sigma$ (purely repulsive interaction between monomers), and $r_c = 2.5\sigma$ (monomer attractions allowed at larger distances). In the course of the study, chain bending stiffness κ and torsional stiffness κ_t were varied by introducing a three-body,

$$V^b(\theta_{ijk}) = \kappa(\cos \theta_{ijk} - 1)^2, \quad (3)$$

and four-body interactions

$$V^t(\phi_{ijkl}) = \kappa_t(1 + \cos \phi_{ijkl}), \quad (4)$$

where θ_{ijk} and ϕ_{ijkl} denote bending and dihedral angle formed respectively by two and three successive bond vectors. In the CG-simulations two kinds of substrates were considered. We employed structureless adsorbing surface (with no friction in the lateral plane), modeled simply by a Lennard-Jones potential acting with strength ϵ_s in the perpendicular z -direction, $V^{\text{sub}}(z) = 4\epsilon_s[(\sigma/z)^{12} - (\sigma/z)^6]$. In a separate set of simulations, we introduced a rough surface composed of beads which form triangular lattice and interact with monomers via Eq. (2) in order to take into account friction between polymer and substrate.

In our simulations we consider, as a rule, the case of strong adsorption $\epsilon_s/k_B T = 5$ and 20 for the structureless surface, and $\epsilon_s/k_B T = 5$ in case of atomistic surface, with T being the temperature of the thermal bath which is described briefly below.

Temperature in our simulations was controlled by two different methods: (i) a Langevin thermostat [16], and (II) by Dissipative Particle Dynamics (DPD) thermostat [17]. In both methods the dynamics of the chain is obtained by solving the following set of equations of motion for the position $\mathbf{r}_n = [x_n, y_n, z_n]$ of each bead in the chain,

$$m\ddot{\mathbf{r}}_n = \mathbf{F}_n^{\text{cons}} + \mathbf{F}_n^{\text{D}} + \mathbf{R}_n \quad (1, \dots, N) \quad (5)$$

with $\mathbf{F}_n^{\text{cons}}$ being the total conservative force acting on each polymer bead with mass $m = 1$.

The influence of the solvent is split into slowly evolving viscous force and rapidly fluctuating stochastic force. Thus, in Eq.(5), \mathbf{F}_n^{D} and \mathbf{R}_n denote respectively the dissipative and random forces which are responsible for keeping the system at constant temperature. The difference between Langevin and DPD thermostats lies in the choice of these two forces.

In the Langevin thermostat, the dissipative force (drag force) is proportional to particle's velocity $\mathbf{F}_n^{\text{D}} = -\gamma_L \dot{\mathbf{r}}_n$, where $\gamma_L = 0.5 m\tau^{-1}$ is the friction coefficient, and the time unit is $\tau = \sqrt{m\sigma^2/\epsilon}$. In addition, the random force has a zero mean value and satisfies the fluctuation-dissipation theorem, $\langle \mathbf{R}_n^\alpha(t) \mathbf{R}_m^\beta(t') \rangle = 2\gamma_L k_B T \delta_{\alpha\beta} \delta_{ij} \delta(t - t')$. These two forces, the random and the frictional one, are balanced in order to maintain the system temperature at the set value.

In contrast to the Langevin thermostat, in the DPD thermostat both dissipative and random forces are applied as pairwise interactions, such that the sum of these two forces acting on a given pair of particle in the system is zero. Thus, in the DPD case the particle momentum is conserved, leading to correct description of hydrodynamic interactions [18, 19]. The form of dissipative and random forces in the case of DPD thermostat is the following: $\mathbf{F}_n^{\text{D}} = \sum_{m(\neq n)} -\gamma_{\text{DPD}} w^2(r_{nm})(\mathbf{r}_{nm}/|\mathbf{r}_{nm}| \cdot \dot{\mathbf{r}}_{nm})\mathbf{r}_{nm}/|\mathbf{r}_{nm}|$ and $\mathbf{R}_n = \sum_{m(\neq n)} \sqrt{2k_B T \gamma_{\text{DPD}}} w(r_{nm}) \alpha_{nm} / \sqrt{dt}$, where the weighting function w is defined as $w(r) = 1 - r/r_c$, $\gamma_{\text{DPD}} = 20 m\tau^{-1}$ is the friction coefficient, and α is a Gaussian-distributed random number with zero mean and variance equal to unity, whereas dt stands for the integration step.

In all CG-simulations the equations of motion were integrated using the MD package LAMMPS [20]. The solvent in our simulations was considered either as being present implicitly via Langevin thermostat or modeled explicitly by adding spherical particles with density $\rho = 0.86 \sigma^{-3}$. In the latter case the difference between Langevin thermostat and DPD thermostat was investigated.

The detachment of chains, composed of $N = 20$, or $N = 100$ monomers, was performed as follows. In the initial state, the chains were completely adsorbed and equilibrated on the surface. The macromolecule was then pulled perpendicular to the adsorbing surface by a cantilever at constant velocity $\mathbf{V} = [0, 0, v_c]$. As a cantilever we used two beads connected by harmonic spring and attached to one of the ends of the chain. The mass of the beads, forming the cantilever, m_c , was set to $m_c = 1$ whereas the equilibrium length of the harmonic spring was set to 0 and the spring constant was chosen as $k_c = 50\epsilon/\sigma^2$. During the pulling simulations, the force $f(t)$ at given height D over the substrate was calculated from the instantaneous harmonic linker extension $\Delta z_l(t)$, i.e., $f(t) = k_c \Delta z_l(t)$.

B. Results

1. Impact of chain properties on the $\langle f \rangle$ - D profile

The saw-tooth response of the pulling force $\langle f \rangle$, measured at any fixed distance D of the chain end above the adsorbing surface, is a characteristic feature produced by the detachment of successive monomers along the polymer backbone, cf. Figure 1a. The observed steady and steep increase of $\langle f \rangle$ after the characteristic last minimum, which corresponds to detachment of the last monomer, is a hallmark of a chain, tethered by one of its ends to the adsorbing substrate and pulled by the other end monomer. It reflects the ultimate extension of the linker spring once all beads,

besides the tethered one, have lost contact with the adsorbing plane. In a real experiment, the chains which have to be detached from the adsorbing surface are most probably not tethered, so the final $\langle f \rangle$ - D profile exhibits instead a sharp drop of the force, which can be also found in our simulations as shown in Figure 1b. This kind of behavior has been observed before for fully flexible homopolymer chains by Jagota *et al.* [10–13] and Paturej *et al.* [14].

Apparently, a semi-stiff tethered chain exhibits the same pattern, (*cf.* Fig. 1a), albeit the ultimate steep growth of the pulling force $\langle f \rangle$ is preceded by a characteristic minimum extending over the last few beads of the chain that precede the tethered bead. Obviously, the last portion of the semi-rigid chain bends and *takes off as a whole*, whereby the length of this chain portion should depend on the chain stiffness. No finite size effect can be detected on Fig. 1a. Indeed, it can be seen that, irrespective of the chain length (either $N = 20$, or $N = 100$), the amplitude and position of the spikes remain insensitive to chain length N . In addition, there is no significant difference between the $\langle f \rangle$ - D profiles for polymer chains adsorbed on a smooth or rough surface (not shown). The only difference is a slightly larger ($\approx 5\%$) amplitude of force $\langle f \rangle$ measured in the case of rough surface.

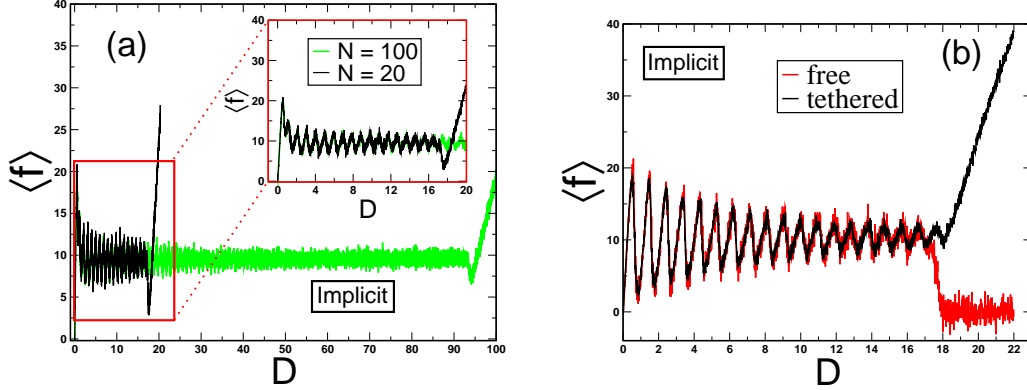


FIG. 1: Short vs long chain desorption in the case of implicit solvent. (a) Mean detachment force $\langle f \rangle$ vs distance D profile is shown for a semi-flexible polymer chain (stiffness parameter $\kappa = 50$). Results pertain to chains composed of respectively $N = 20$, and 100 monomers. For better visibility, the onset of the desorption process is zoomed in the inset. (b) Detachment of a chain whose end is *not* tethered to the substrate. In both figures $\epsilon_s/k_B T = 20$ and $v_c = 10^{-3} \sigma/\tau$.

Generally, one may speculate how the chain stiffness affects the $\langle f \rangle$ vs D diagram. The bending stiffness of the polymer backbone was included in the simulation by allowing for the three-body bending potential, $V_b(\theta)$, where θ is the angle between two consecutive bonds, *cf.* Eq. (3). The stiffness parameter κ determines the persistence length of the chain, l_p , which is defined through the decay of bond angle correlations [21]. Figure 2 shows simulation results for different stiffness parameter κ and chain length N .

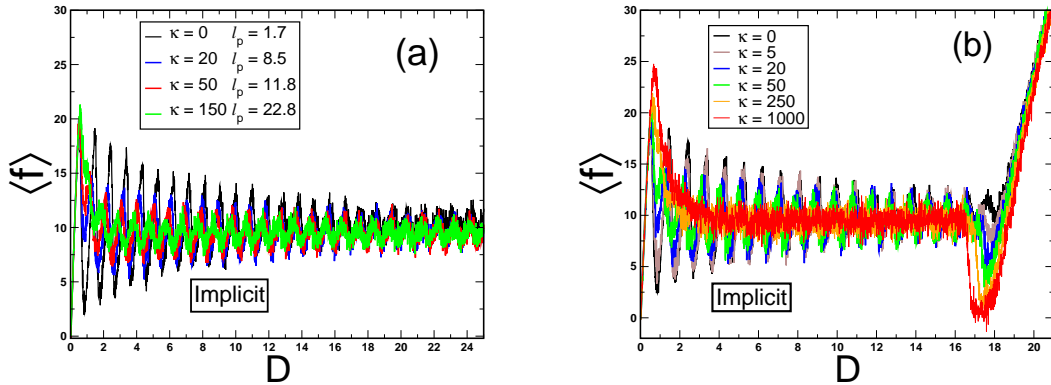


FIG. 2: Force-distance diagram for semiflexible chains in implicit solvent. Stiffness parameter κ and persistence length l_p are indicated in the legend: (a) Chain length $N = 100$. With growing stiffness κ the spikes amplitude *decreases*. (b) Chain length $N = 20$. The end of the detachment process is marked by a force minimum which becomes more pronounced with growing stiffness. Here $\epsilon_s/k_B T = 20$ and $v_c = 10^{-3} \sigma/\tau$.

It can be seen that with growing stiffness, the amplitude of the spikes decreases and also the spikes resolution

deteriorates. Starting with approximately $\kappa = 50$, the complete chain detachment is preceded by a characteristic force minimum (in case of tethered chains). Then, with growing stiffness κ this minimum, which marks the ultimate chain detachment, occurs at smaller D , indicating that increasingly larger portions of the polymer backbone are detached as a whole. The minimal detachment force thereby also drops so that at $\kappa = 1000$ it approaches zero. However, for realistic values of the stiffness κ , and not extremely short chains, $N \geq 10$, the total energy, E_{rod} , needed for tearing off the polymer as a single piece of rod from the adsorbing plane, $E_{rod} \propto N\epsilon_s$, would be huge in comparison to the energy, E_{arc} , needed to tear off the same semi-flexible chain bead by bead, $E_{arc} \approx n_m\epsilon_s + (n_m - 1)\kappa\theta_b^4$, with few beads n_m that form an arc of the bended portion of the chain backbone, Fig. 3. Once an arc is formed, no further energy penalty will be needed to keep the chain bended during the rest of the detachment process.

A rough estimate, using the potential $V^b(\theta)$, Eq. (3), with $\theta = 10^\circ$ degrees yields $\kappa \times 5.310^{-8}$ bending energy per bond, or $E_{arc} \approx 10^{-5} k_B T$ for an arc encompassing 10 bending angles and $\kappa = 100 k_B T$. In the same time such an arc can already reach a height of $10 \times \cos(10^\circ)\sigma \approx 1.74\sigma$, where surface adhesion is already dwindling. Therefore, the detachment of even rather stiff chains instantaneously as a rod-like object should be ruled out and a $\langle f \rangle$ - D profile of the type, shown in Figure 2, is likely to be observed.

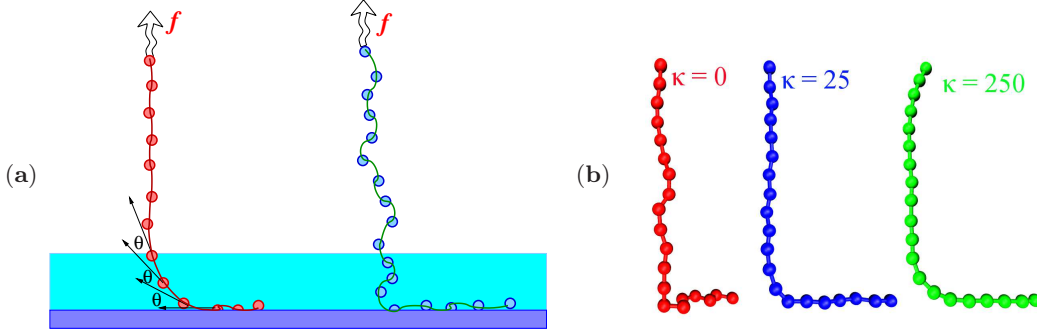


FIG. 3: (a) Schematic picture of a force-induced detachment of a semi-stiff (left) and flexible (right) chain from a solid plane. The bending angle θ between successive bonds is indicated. Light-shaded area denotes the range of the adsorption potential $V^{sub}(z)$. (b) Snapshots of partially detached polymer chains of different stiffness κ as indicated. In each case 66% monomers were peeled off the substrate.

Owing to the creation of arc, more than one bead detach concertedly and move away from the adhesive surface beyond the range of adsorption. The neighboring beads along the arc, i and j , remain thereby at fixed mutual distance $z_{ij} < \sigma$. The neighboring bonds slightly bend but do not stretch significantly so that the length of the individual bond is close to the unperturbed length yet much less than the maximal one, $r_0 = 1.5\sigma$, cf. Eq. (1). As a result, depending on chain stiffness and in contrast to flexible chains, the monomers in a semi-stiff chain detach concertedly rather than one by one which exerts a smearing effect on the saw-tooth diagram $\langle f \rangle - D$, Fig. 2a. Increasing bending stiffness also decreases the magnitude of saw-tooth profile amplitude as the bonds between neighboring monomers stretch less.

Realistic DNA-models usually include also a dihedral potential which is responsible for the chain resistance to torsion. We have used the dihedral potential, $V_t(\phi)$, where ϕ is the dihedral angle and the torsion constant is $\kappa_t = k_B T$, Eq. (4). The resulting $\langle f \rangle$ vs. D diagram for a chain with torsional and bending finite stiffness, compared to the fully flexible, and semi-flexible ($\kappa = 50$) chain models, is shown in Fig. 4. It can be seen that while the bending stiffness itself leads to a clear shift of the force oscillation pattern, the resulting behavior practically does not change upon inclusion of a dihedral potential.

2. Effects of substrate adhesion on polymer detachment

It is to be expected that the strength of adhesion of the polymer chain to the adsorbing surface will manifest itself in the recorded variation of desorption force $\langle f \rangle$ with distance D . While in the previous graphs, Figures 1-4, we focused on cases of strong adsorption, $\epsilon_s = 20k_B T$, in Figure 5a we present the desorption profile for weak to moderate attraction of the chain by substrate (in our model the threshold for adsorption $\epsilon_s^{crit} \approx 3k_B T$). Indeed, as indicated in Figure 5a, at $\epsilon_s = 5k_B T$, the characteristic oscillations in the $\langle f \rangle$ - D profile virtually vanish (apart from the statistical noise). Therefore, one may conclude that the method of single chain detachment spectroscopy as a tool for sequencing analysis could be used in cases of strong polymer - substrate adhesion only.

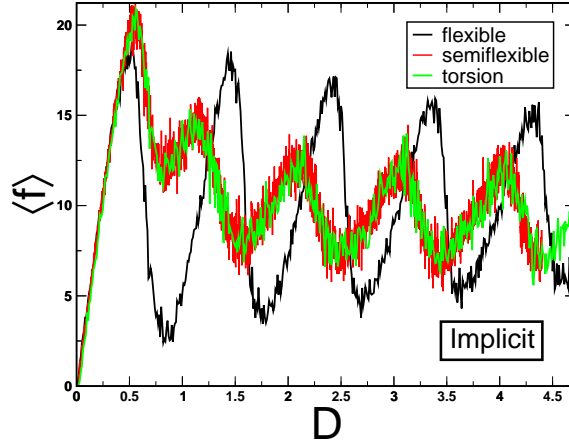


FIG. 4: Force $\langle f \rangle$ vs D diagram for flexible, semiflexible and torsional (angle and dihedral potential included) as indicated. Here $N = 20$, $\epsilon_s/k_B T = 20$, $v_c = 10^{-3} \sigma/\tau$, $\kappa = 50 k_B T$ and $\kappa_t = k_B T$.

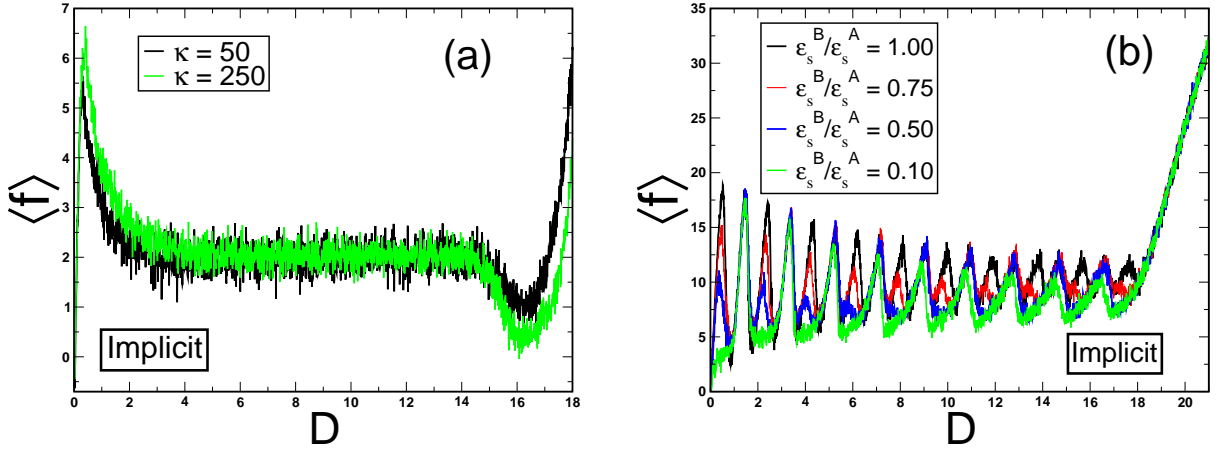


FIG. 5: (a) Force $\langle f \rangle$ vs D diagram of a homopolymer for attraction strength of the surface $\epsilon_s = 5k_B T$ and two different values of the bending stiffness, $\kappa = 50, 250 k_B T$. (b) The same for alternating copolymers made of two types of monomers A and B which have different binding energies to the substrate, ϵ_s^A and ϵ_s^B , respectively. Results are displayed for different ratios $\epsilon_s^B/\epsilon_s^A$ as indicated in the legend. The case of $\epsilon_s^B/\epsilon_s^A = 1$ corresponds to a homopolymer. The absolute value of ϵ_s^A here is $20 k_B T$. In both figures $N = 20$ and $v_c = 10^{-3} \sigma/\tau$.

For the objectives of sequencing, the legibility of the data, derived by this method of force-induced detachment, must be examined for heterogeneous polymers in particular. As an example, the result for an alternating ($A - B$)-copolymer detachment is shown in Figure 5b. Here monomers A and B have different affinity to the substrate (albeit the same mass $m_A = m_B$). The detachment starts with a B -monomer (i.e., a monomer with a relatively smaller affinity to the substrate). For a ratio of $\epsilon_s^B/\epsilon_s^A = 0.5$, the alternating pattern of spikes can still be clearly seen. As ϵ_s^B gradually further declines, the set of force maxima, corresponding to the desorption of B -monomers, decreases significantly in amplitude. Eventually, for $\epsilon_s^B/\epsilon_s^A = 0.1$, the maxima corresponding to tearing-off B -monomers turn into minima. Moreover, the latter effect is observed even at higher values of the $\epsilon_s^B/\epsilon_s^A$ -ratio once the first few repeating units are detached. So at larger height D of the pulled chain end (approximately starting from $D = 8\sigma$), for the B -type monomer desorption one observes local minima rather than peaks. Evidently, a correct sequencing of heterogeneous macromolecules can be performed only in cases when the affinity of the various building blocks is large in terms of absolute values of binding energy ($> 10 k_B T$) and the differences between values of binding energy should be significant.

3. Implicit vs. explicit solvent

So far we examined how the force-displacement profile of different polymer chains reflects the properties of the chains and their interaction with the adsorbing surface. It is of some interest to check whether the properties of the surrounding medium, considered in the different simulation setups, might influence the $\langle f \rangle$ - D profile too.

In many computational experiments, as e.g. in our previous publication [14], one takes the solvent only implicitly into account. The solvent properties can be then varied to a limited amount only, for example, by changing the friction coefficient γ in Eqs. (5). In principle, however, the presence of an explicit solvent might affect the course of force-induced chain desorption due to hydrodynamic interactions (HI). To this end we compare the $\langle f \rangle$ vs D diagram, derived from simulations of the same system when two different thermostats are used: (i) a Langevin thermostat (i.e., with no HI), and (ii) a DPD thermostat. It is well known that the latter allows for a correct hydrodynamic behavior [18, 19], whereas the Langevin thermostat does not exhibit momentum conservation, and therefore does not reproduce the proper hydrodynamic behavior. In the case of explicit solvent, a chain is pulled in a Lennard-Jones liquid with liquid monomer density $\rho = 0.86\sigma^{-3}$.

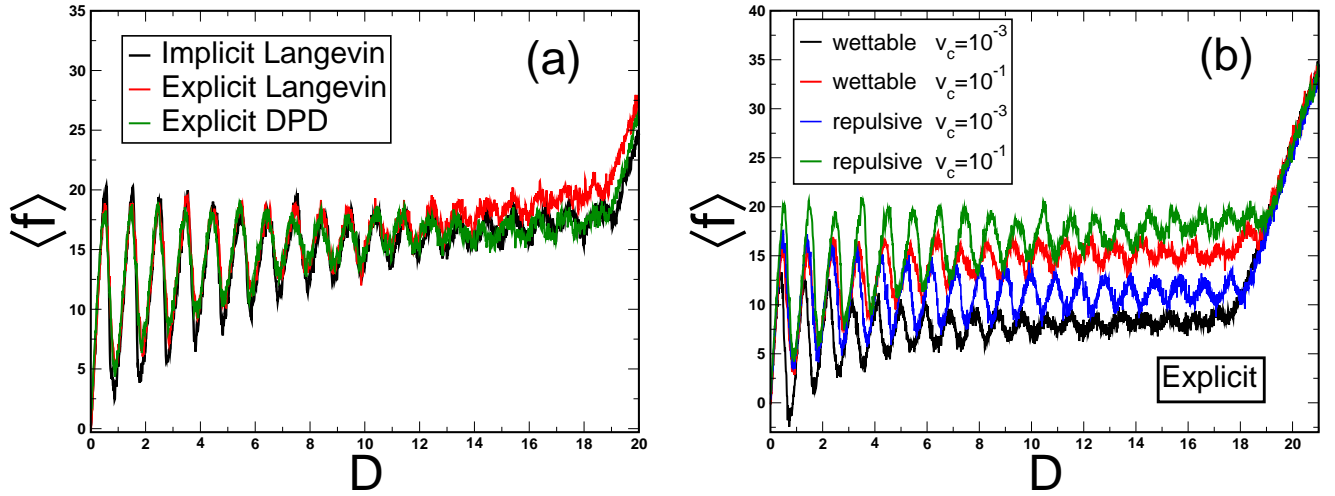


FIG. 6: (a) Comparison of the force $\langle f \rangle$ vs D diagram for implicit and explicit solvents from simulations with Langevin, and DPD thermostats, respectively. Results are presented for fast pulling, $v_c = 10^{-1} \sigma/\tau$. (b) Impact of the substrate selectivity for the case of explicit solvent and DPD thermostat. Force $\langle f \rangle$ vs. displacement D diagram for wettable and solvophobic substrates at two pulling velocities. In both figures $N = 20$ and $\epsilon_s/k_B T = 20$.

It is evident from Figure 6a, however, that there is no tangible difference between these cases, which suggests that the hydrodynamic interaction is largely irrelevant in detachment experiments. In fact, when compared to the case of explicit solvent with no HI (Langevin thermostat), the presence of HI (accounted for by DPD) leads to a slight decrease in the pulling force, cf. Figure 6a, at the end of the detachment process. Evidently, this affects the detachment of the last beads only while the main portion of the chain is sufficiently far away from the substrate. While such an effect is completely missing for slow detachment with $v_c = 10^{-3} \sigma/\tau$ (not shown here), for fast detachment, $v_c = 10^{-1} \sigma/\tau$, it should actually be expected due to the solvent back-flow, triggered by Stokes friction of the detached chain portion when the desorbed chain eventually sets into motion. Moreover, due to confinement effects, HI (being long-ranged) are screened [27] in the vicinity of the adhesive wall, which explains why their presence is detectable only at sufficiently large distance D from the wall. Therefore, one can view the small decrease in $\langle f \rangle$ in the case of explicit solvent as a typical manifestation of the well-known difference between Rouse and Zimm dynamics of polymers.

4. Substrate wettability

We checked also to what extent the affinity of the adsorbing substrate with respect to solvent plays a role. Basically, we distinguish between *solvophobic* (repulsive) substrates, where the polymer chain is still attracted to the surface whereas the solvent particles are repelled, and *wettable substrates*, where both the polymer and the solvent are attracted to the surface. Figure 6b indicates a systematic decrease in the amplitude of the spikes for wettable substrates (as if the solvophobic solvent effectively increases the chain adhesion to the surface), yet the characteristic saw-tooth force

vs distance profile remains qualitatively unchanged. The spikes positions under conditions of good wetting are also slightly shifted to lower values of D , i.e., the monomers detach more easily (at somewhat lower height) as compared to the solvophobic case. This is because as the relative attraction of solvent particles to the surface is increased, the solvent particles try to replace chain monomers and form a solvent layer on the surface, which in turn, facilitate the desorption of chain monomers. In the context of protein-surface interactions, this effect is referred to as *Berg limit* and was also observed in the simulations of biopolymers on various hydrophobic/philic surfaces by Schwierz *et al.* [32].

5. Desorption at different temperature

Eventually, we examined the role of temperature T in the process of chain detachment and its impact on the force-displacement diagram. T (measured in units of the monomer - monomer interaction strength ϵ/k_B) was increased, while the adsorption strength ϵ_s was also correspondingly changed so as to keep the ratio $\epsilon_s/k_B T$ constant and equal to $\epsilon_s/k_B T = 20$ as in most of the presently studied cases. The presence or absence of explicit solvent revealed thereby almost no difference again.

Expectedly, the mean level of the force (the average plateau height) grows, reflecting the stronger adhesion ϵ_s , while, surprisingly, the amplitude of the spikes remains largely unchanged. A simple explanation for this observation

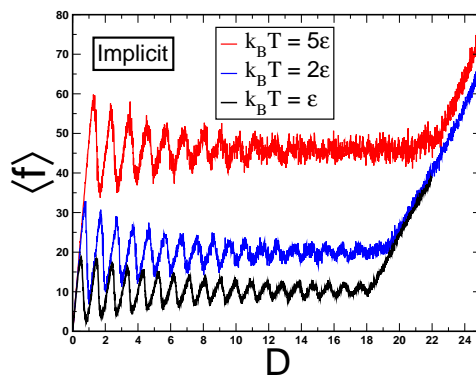


FIG. 7: (a) Comparison of pulling results performed at different temperatures T (see legend) and constant ratio $\epsilon_s/k_B T = 20$ and $N = 20$.

in the force detachment experiment can be suggested as follows.

We consider the chemical potential of adsorbed, μ_{ads} , and detached segments, μ_{det} , which should become equal on the detachment line, i.e., $\mu_{\text{ads}} = \mu_{\text{det}}$. In the limit of strong adsorption (or, at low temperature), when the macromolecule is tightly bound to the surface and loops (non-adsorbed chain portions) may be neglected, the free energy gain (per chain segment) upon adsorption reads:

$$\mu_{\text{ads}} = \underbrace{-\epsilon_s}_{\text{energy gain}} - k_B T \underbrace{\ln(\mu_2/\mu_3)}_{\text{entropy loss}} \quad (6)$$

In Eq. (6) ϵ_s again stands for the adsorption energy of a single segment while μ_2 and μ_3 are the so called *connective constants* in two- and three dimensional space respectively. The latter correspond roughly to the possible orientations of a chain segment in space, i.e., the logarithms thereof yielding effectively the entropy contributions in two- and three-dimensions. It has been shown that for cubic lattices, for instance, $\mu_2 = 2.6$ and $\mu_3 = 4.68$ [28].

On the other hand, in the limit of strong adsorption, the detached chain portion is strongly stretched, attaining a “string” configuration, so that the elastic free energy per segment reads $\mu_{\text{det}} = -af$, where a is the Kuhn length and f is the force acting on the chain end. Moreover, in the “string” state a segment has only one orientation, i.e. $\mu_3 = 1$. On the $\langle f \rangle - D$ plateau, $f = f_p$, and due to the condition $\mu_{\text{ads}} = \mu_{\text{det}}$ one has the following “plateau”-relationship

$$af_p = \epsilon_s + k_B T \ln \mu_2 \quad (7)$$

This result shows that for a strong adsorption the plateau height (i.e., the pulling force) is proportional to the adsorption energy. The result given by Eq. (7) has been obtained first within a more general consideration in our paper [29] (see Eq. (30) in [29]). This is now supported by Figure 7 where the temperature and adsorption energy are changed proportionally to one another.

The $\langle f \rangle - D$ diagram demonstrates in all cases the characteristic saw-tooth behavior with the amplitude progressively decaying in the course of chain detachment. This behavior has been analyzed first by Jagota *et al.* [10]. In terms of the number of detached chain segments, the n -th spike correspond to the reversible transition $n \leftrightarrow n + 1$ during which the detachment of a segment leads to release of polymer stretching energy back to the energy of adsorption ϵ_s . This condition leads to the spikes amplitude law [10]

$$f_{\text{amp}} \sim \exp[(\epsilon_s/k_B T - \ln 4\pi)/n]. \quad (8)$$

This relationship is clearly in line with the decay behavior upon growing n . On the other hand, provided that the temperature and adsorption energy are increased proportionally to each other, the spikes amplitude does not change. That is exactly what we observe in Figure 7.

Figure 7 also shows that the overall elastic modulus of the tethered chain does not depend on temperature. Most probably, this is due to the fact that for the strong stretching the entropic contribution to elastic modulus (modulus grows with temperature) is compensated by the bond anharmonicity effect when the elastic modulus decreases with temperature.

III. ALL-ATOM SIMULATIONS

A. Model

It appears instructive to compare the obtained simulation results for a coarse-grained model to those for an atomistic model of a concrete macromolecule. The latter were performed with the Gromacs MD package [4] using the Gromos96 force field [22] and the SPC/E (Single Point Charge/Extended) water model [23] at constant surface area A and at constant vertical pressure P_z of 1 bar with temperature $T = 300$ K. For the temperature and pressure control, the method of Berendsen [24] was used. Periodic boundary conditions for the Coulomb interactions were implemented by the particle-mesh Ewald method [25]. Simulation runs were performed with an integration time step equal to 2 fs.

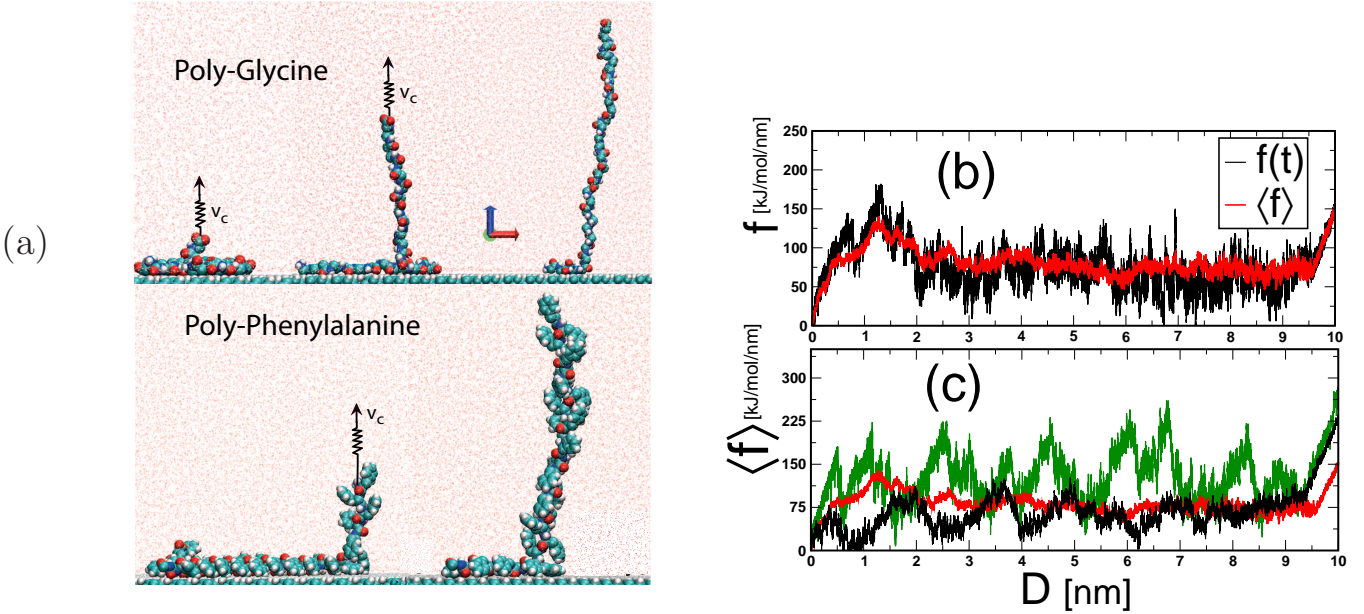


FIG. 8: *Biomolecule (polypeptide) desorption.* (a) Vertical pulling of 31-glycine and 31-phenylalanine chains adsorbed on hydrophobic diamond surface. Small red dots represent water molecules. (b) Force $\langle f \rangle$ vs D diagram for 31-glycine desorption. Red line represents an average over 25 simulated desorption events whereas the black line shows a single run simulation data. (c) Averaged force $\langle f \rangle$ vs D diagrams for: 31-glycine (red line), 6-(Gly-Gly-Gly-Gly-Phe) (black line) and 31-phenylalanine (green line). Here $k_c = 200$, $\epsilon_s/k_B T \approx 7$ and the pulling velocity $v_c = 1$ m/s.

The simulation box contains a hydrophobic diamond slab with a water-surface contact angle $\theta_c \approx 90^\circ$ [30], a single $N = 31$ amino acid (AA) chain, and ca. 16000 SPC/E water molecules. The entire system, including diamond surface,

is composed of 70000 atoms. Dimensions of the simulation box are around $7\text{ nm} \times 7\text{ nm} \times 12\text{ nm}$, and the thickness of a diamond slab is 1.8 nm. The ratio between adsorption strength of the surface and thermal energy is around 7 – 10. This binding energy is of the order of the binding energy 8.3 ± 0.7 of polythymine 3'poly(dC₅₀) on graphite substrate [11]. For the hydrophobic surface, the $\langle 100 \rangle$ -plane of an elastic diamond substrate is saturated completely by uncharged hydrogen atoms. The peptide is allowed to adsorb on the surface prior to solvation by water. After equilibration of the chain on the surface, the pulling is performed, cf. Figure 8a, whereby initially the molecule is completely adsorbed on surface.

Similar to CG simulations, the molecules were pulled via a harmonic linker attached to one of the ends of the molecule as shown in Figure 8. The harmonic spring is moved vertically at a prescribed velocity v_c until the entire chain is desorbed from the surface. The spring exerts no lateral force on the chain, and the chain can move freely on the surface. The spring constant is chosen as $k_c = 300\text{ pN/nm}$. The force needed to pull the peptide vertically is calculated via $F = k_c(v_c t - z_t)$, where z_t is the z -component of the position of the terminal amino acid. The velocity is taken as $v_c = 1\text{ m/s}$, which has been demonstrated earlier to provide a quasi-equilibrium pulling on the corresponding surface [26].

Indeed, a pulling velocity $v_c \lesssim 1$ can also be justified by scaling arguments borrowed from the polymer physics: When HI is included, the relaxation time of chain with N Kuhn monomers is $\tau_Z \approx N^{3\nu} \tau_0$ [21], where the scaling exponent $\nu \approx 3/5$ for good solvent, $\tau_0 \approx a^2 \gamma_0 / k_B T$ is the relaxation time of a Kuhn segment with a monomeric friction coefficient in the solvent γ_0 . If τ_Z is smaller than the time scale imposed by the pulling $\tau_c \approx a / v_c$, i.e., $v_c \lesssim v_c^* \equiv k_B T / a N^{3\nu} \gamma_0$, the undesorbed section of the chain will be in quasi-equilibrium for which pulling forces should not depend on the conformation of the remaining chain section on the surface. If we take the Kuhn segment size (twice the persistence length) of an AA chain as $a \approx 1\text{ nm}$ (i.e., 1-3 AA monomers), $N \approx 10$ and a monomeric friction coefficient of $\gamma_0 \approx 10^{-12}\text{ kg/s}$ for the diamond surface [31] and $k_B T \approx 4 \times 10^{-21}\text{ kgm/s}^2$, we obtain a threshold velocity $v_c^* \approx 1\text{ m/s}$. Note that v_c^* will be much lower if the monomeric friction coefficient is $\gamma_0 \gg 10^{-12}\text{ kg/s}$, e.g. for a OH saturated surface [31] or if the chains are longer.

Above argument for the chain relaxation on the atomistic surface also applies to our CG simulations since in most of our CG simulations (except for the rough surface), the pulled chains interact with the surface only via a z -dependent potential. This means that chains can laterally diffuse on the surface but with a bulk diffusion coefficient (see Section II.A).

B. Comparison with Coarse-Grained simulations

The all-atom simulations of polypeptide desorption from atomistically rough substrate were performed for a $N = 31$ polyglycine (31-glycine), $N = 31$ polyphenylalanine (31-phenylalanine). We also constructed a $N = 31$ hetero-peptide composed of six (Gly-Gly-Gly-Gly-Phe) groups, where Gly and Phe stand for glycine and phenylalanine monomers, respectively.

The results for 31-glycine chain desorption are presented in Figure 8b along with several snapshots from different stages of the desorption event. The snapshots taken from 31-glycine pulling trajectories compare well to those obtained from coarse-grained simulations shown in Fig. 3. Comparing the first few spikes in Figure 8b and in Figure 4, the general pattern resembles much more the saw-tooth profile, typical for semi-rigid, rather than for completely flexible polymers, in line with the nature of this polypeptide. Although the data for the $\langle f \rangle$ - D diagram, shown in Figure 8b, are averaged over 25 simulation runs only and appear somewhat noisy, they reveal a characteristic $\langle f \rangle - D$ behavior, which qualitatively complies with the results from our coarse-grained simulation. Due to the relatively short length of this glycine macromolecule, the final 'dip' before contact with the adhesive substrate is lost, is rather short yet clearly visible as in the CG $\langle f \rangle$ - D diagrams of tethered chains.

To compare 31-glycine force trace with a stiffer chain, desorption simulations of 31-phenylalanine (red data in Figure 8c) were performed. As seen in Figure 8c, the saw-tooth peaks are more visible, and the peak-forces are much higher than those observed for 31-glycine cases. This is actually due to the large benzyl side chain of phenylalanine monomers: The hydrophobic nature of the side chain increases the affinity of phenylalanine monomers to the hydrophobic surface, hence, results in higher force peaks. Interestingly, visual inspection of our simulation trajectories revealed that the benzyl side chains force the overall 31-phenylalanine molecule to take a rod-like structure on the surface (see the snapshot in Figure 8a). However, the pulling snapshots shown in Fig. 8a show that the conformation of 31-phenylalanine during the pulling resembles more that of the 31-glycine rather the illustration shown in Fig. 3 for the CG model with $\kappa \gg 25$. We attribute this to the similar atomistic AA backbone structure of both chains.

The $\langle f \rangle$ - D diagram of our hetero-peptide chain composed of (Gly-Gly-Gly-Gly-Phe) groups is shown in Figure 8c (black data). One can distinguish individual desorption peaks for 6 phenylalanine monomers separated by peel-off's of glycine monomers which is also observed in CG simulations of alternating polymers (see Figure 5b). The

phenylalanine-induced force peaks observed in the force trace of hetero-peptide chain are lower than those observed for the 31-phenylalanine chain itself. This 2-fold difference in the peak forces can be due to complex interplay of chain stiffness and the relative surface affinity of monomers with respect to neighboring monomers: Possibly, glycine monomers might decrease the adsorption energy of adjacent phenylalanine monomers since they can diffuse faster due to their relatively small sizes (the side chain of a glycine is one hydrogen). This observation in Fig. 8c hints that the adsorption energy per AA residue can have a dependence on sequence and deserves further investigation in future. Also note that the maxima of saw-tooth in Fig. 5b for CG model show a tendency to decrease as the adhesion asymmetry of alternating monomers grows.

Overall, by comparing CG and atomistic simulations, one may conclude that the coarse-grained modelling of force-induced desorption of a polymer chain from adhesive substrate agrees well with the results from all-atom simulations.

IV. SUMMARY

In the present investigation we studied the process of polymer chain detachment by an external force, applied to the end-segment of a semiflexible chain which is strongly adsorbed to adhesive substrate. Most of the results have been derived by means of Molecular Dynamics simulations of a coarse-grained bead-spring model of a polymer chain, and focused on the analysis of the recorded (fluctuating) mean force $\langle f \rangle$ at height D of the last segment of the chain above the adsorbing plane when the segment is pulled with given velocity v_c . As a principal objective of this investigation, the influence of different parameters that characterize the polymer chain, its adhesion to the substrate, and the substrate - solvent affinity on the ensuing $\langle f \rangle$ - D diagram have been examined.

We have found that an increasing bending rigidity of the polymer induces a sharp drop of the pulling force *before* the last segments of the chain are peeled off, i.e., the final portion of the chain is detached as a single piece of rod. Nonetheless, our observations and estimates suggest that the sequential desorption of polymer repeatable units from the substrate retains its characteristic “unzipping” mechanism, reflected by the observed “saw-tooth” $\langle f \rangle - D$ profile, up to very high degree of rigidity. This mechanism works not only for fully flexible chains but also for rather stiff ones due to the gradual bending of the macromolecule which is energetically much more favorable.

We also find that with increased bending stiffness κ , the modulation of the characteristic oscillatory profile steadily declines, similar to the effect of weaker attraction ϵ_s of the chain to the adsorbing surface where the spikes vanish already at $\epsilon_s \approx 5k_B T$. In contrast, the torsional stiffness of the polymer has little or no effect of the $\langle f \rangle$ - D diagram.

Regarding the possible use of the $\langle f \rangle$ - D diagram for sequencing and its legibility, the performed detachment of an $A - B$ -copolymer indicates that the ratio $\epsilon_s^B / \epsilon_s^A$ of binding energies of the A - and B -segments strongly influences the resulting oscillatory profile so that when $\epsilon_s^B / \epsilon_s^A < 10\%$ the spikes that refer to B -atoms practically disappear.

Our studies indicate that the role of hydrodynamic interactions (HI) in the process of forced-induced detachment of a macromolecule from adsorbing surface is negligible. The resulting $\langle f \rangle$ - D diagrams, emerging from MD simulations with and without explicit solvent, hardly warrant the incomparably larger computational efforts in the former case. This insensitivity of the problem regarding HI is related most probably to the resulting stretched conformation of the pulled macromolecule, and to the effect of screening of HI in the vicinity of the adsorbing surface.

Eventually, by comparing our data derived from a coarse-grained bead-spring model of a macromolecule to data from a realistic all-atom simulation of various bio-polymer (e.g., glycine, phenylalanine), peeled off a hydrophobic diamond substrate, we have demonstrated that the observed $\langle f \rangle$ - D diagrams agree qualitatively well with each other, underlying thus the relevance of coarse-grained computer modelling.

Acknowledgments

This research was supported by the Polish Ministry of Science and Higher Education grant *Inventus Plus* Project No.: IP2012 005072.

-
- [1] R. Merkel, *Phys. Rep.* **2001**, 346 , 343 .
 - [2] F. Ritort, *J. Phys.: Condens. Matter* **2006**, 18, R531.

- [3] I. Franco, M.A. Ratner, G.C. Scatz, Single-Molecule Pulling: Phenomenology and interpretation, in *Nano and Cell Mechanics: Fundamentals and Frontiers*, edited by H.D. Espinosa and G. Bao (Wiley, Microsystem and Nanotechnology Series, 2013, ch. 14, pp. 359-388).
- [4] Lindahl, E.; Hess, B.; van der Spoel, D. *J. Mol. Model.* **2001**, *7*, 306317
- [5] G.I. Bell, *Science* **1978**, *200*, 618.
- [6] E. Evans, K. Ritchie, *Biophys. J.* **1997**, *72*, 1541.
- [7] E. Evans, *Annu. Rev. Biophys. Biomol. Struct.*, **2001**, *30*, 105.
- [8] A.M. Baró, R.G. Reifenger (editors), *Atomic Force Microscopy in Liquid: Biological Applications*, Wiley-VCH Verlag & Co. KGaA, Weinheim, 2012.
- [9] R. Merkel, P. Nassoy, K. Ritchie, E. Evans, *Nature* **1999**, *397*, 50 .
- [10] S. Manohar, A. Jagota, *Phys. Rev. E* **2010**, *81*, 021805.
- [11] S. Manohar, A.R. Manz, K.E. Bancroft, Ch-Y. Hui, A. Jagota, D.V. Vezenov, *Nano. Lett.* **2008**, *8*, 4365.
- [12] S. Iliafar, D.V. Vezenov, A. Jagota, *Langmuir* **2013**, *29*, 1435.
- [13] S. Iliafar, K. Wagner, S. Manohar, A. Jagota, D.V. Vezenov, *J. Phys. Chem. C* **2012**, *116*, 13896.
- [14] J. Paturej, J.L.A. Dubbeldam, V.G. Rostiashvili, A. Milchev, T. Vilgis, *Soft Matter* **2014**, *10*, 2785.
- [15] K. Kremer and G.S. Grest, *J. Chem. Phys.* 1990, *92*, 5057
- [16] T. Schneider and E. Stoll, *Phys Rev B* 1978, *17*, 1302
- [17] R. D. Groot and P. B. Warren, *J. Chem. Phys.* 1997, *107*, 4423
- [18] I. Pagonabarraga, M. H. J. Hagen and D. Frenkel, *EPL* 1998, *42*, 377
- [19] T. Sodemann, B. Dünweg and K. Kremer, *Phys. Rev. E* 2003, *68*, 046702
- [20] S.J. Plimpton, *J. Comp. Phys.* 1995 *117*, 1.
- [21] A. Yu. Grosberg, A.R. Khokhlov, *Statistical Physics of Macromolecules*, AIP Press, New York, 1994.
- [22] W. R. P. Scott, P. H. Hünenberger, I. G. Tironi, A. E. Mark, S. R. Billeter, J. Fennen, A. E. Torda, T. Huber, P. Krüger, W. F van Gunsteren, *J. Phys. Chem. A* **1999**, *103*, 3596.
- [23] H. J. C. Berendsen, J. R. Grigera, and T. P. Straatsma, *J. Phys. Chem* **1987**, *91*, 6269
- [24] , K. A. Feenstra, B Hess, H. J. S. Berendsen *J. Comput. Chem.* **1999**, *20*, 786.
- [25] T. Darden, D. York, L. Pedersen *J. Chem. Phys.* **1993**, *98*, 10089
- [26] D. Horinek, A. Serr, M. Geisler, T. Pirzer, U. Slotta, S. Q. Lud, J. A. Garrido, T. Scheibel, T. Hugel, R. R. Netz *Proc. Natl. Acad. Sci. U.S.A.* **2008**, *105*, 2842
- [27] A. Winkler, P. Virnau, K. Binder, R. G. Winkler, and G. Gompper, *Europhys. Lett.* **2012**, *100*, 46003
- [28] C. Vanderzande, *Lattice Model of Polymer*, Cambridge University press, Cambridge, 2004.
- [29] J. Paturej, A. Milchev, V.G. Rostiashvili, T.A. Vilgis, *Macromolecules* **45**, 4371 (2012).
- [30] F. Sedlmeier et al. *Biointerphases* **2008**, *3*, 2339
- [31] A. Erbas, D. Horinek, R.R. Netz, *J. Am. Chem. Soc.* **2012**, *134*, 623
- [32] N. Schwierz et al. *J. Am. Chem. Soc.* **2012**, *134*, 1962819638